Performance Analysis of Axial-Flow Mixing Impellers

Jie Wu and Lionel Pullum
Advanced Fluid Dynamics Laboratory, Commonwealth Scientific and Industrial Research Organisation, Highett, Victoria 3190, Australia

Theoretical formulations for impeller performance were evaluated based on a blade-element theory. These enable the calculation of the head and power vs. flow-rate curves of axial-flow impellers. The technique uses the lift and drag coefficients of the blade section of an impeller to calculate the spanwise swirl-velocity distribution. Using the angular-momentum equation, it is possible to calculate the corresponding spanwise distribution of the energy head of the impeller. Integration of these distributions of head and torque gives the impeller's performance. Parameters including the flow number, the power number, the thrust force number, and the swirl velocity can be found at the impeller operating point, determined using the head curve and an experimentally calibrated resistance curve. A laser Doppler velocimetry (LDV) system was used to measure the velocity distribution for different axial flow impellers in mixing tanks. Calculated flow and power numbers agreed well with the experimental results. Using the blade's spanwise head distribution and a set of calibrated flow-resistance data, it is also possible to estimate an impeller's outlet axial-velocity distribution. Predictions compared well with LDV experimental data. The effect of impeller-blade angle, number of blades, blade camber, and blade thickness on the performance of axial-flow impellers was investigated using the Agitator software.

Introduction

Mixing with impellers in a vessel is a common technique found in many process industries, and there is a wealth of literature describing mixing-vessel impeller characteristics. Jaworski et al. (1991), using a laser Doppler velocimetry (LDV) system, measured the velocity field in a mixing vessel agitated by a 45° pitched-blade turbine. They determined the impeller flow number using the mean flow-velocity data. The flow number was found to change slightly with change in impeller-to-tank-bottom clearance. Weetman and Oldshue (1988) presented correlations for power, flow, and shear characteristics of many different impellers, measured through an automated LDV system. The impellers examined by their study ranged from highly efficient axial-flow impellers to radial impellers that produce high shear rates. Similarly, Lee and Yianneskis (1998), Nouri and Whitelaw (1990), and many others have presented the flow field and impeller characteristics through similar measurements. Yianneskis et al. (1987) showed detailed flow structures of the tip vortices attached to Rushton turbine, using LDV techniques. Using a novel image-shifting technique, Wu et al. (1997) visualized the flow field in the frame of reference rotating with the impeller. Tip vortices and separation bubbles along the blades were identified.

The fluid flow in a mixing vessel is primarily a function of the fluid rheology, tank geometry, and the design and operation of the impellers. The relationship between the energy head developed by the impeller, torque, power, hydraulic efficiency, and the impeller flow rate, which will be referred to as performance curves, are fundamental to understanding and predicting a system's operation.

Traditionally, characterization of an impeller using its performance curves has been widely used in the fan industry, gas turbine industry, and pump industry (Wallis, 1983; Downie et

Correspondence concerning this article should be addressed to J. Wu.

al., 1993; Lewis, 1996). Performance analysis of impellers for pumps or fans is crucial in determining fluid velocity, impeller power, duct pressure, and other design parameters. Downie et al. (1993) developed a computer program for the design and evaluation of the performance of low- to medium-pressure axial-flow fans, based on blade-element theory developed by Wallis several decades earlier (Wallis, 1983). Using this program, they were able to estimate the effect on fan performance of varying impeller geometry, including impeller-blade setting angle, blade solidity, and blade shape. They demonstrated the accuracy of the program by comparing the predictions with experimental data obtained from measurements using a model fan test facility.

Performance analysis of impellers in mixing has not received nearly the amount of attention as has the fan, gas turbine, and pump industries. While it is possible to use computational fluid dynamics (CFD) to solve the full three-dimensional velocity field in mixing tanks (Hutchings et al., 1989; Weetman, 1991), in order to evaluate the performance of an impeller, CFD solution for mixing-tank flow is usually computing intensive. A full accurate solution of the mixing-tank flow requires solving not only the large-scale mixing-tank velocity field but also the fine boundary layer and the tip vortices developing along the blades of the impeller. Automated sliding mesh computations are usually required for this approach (Koh and Wu, 1998; Weetman, 1997).

The objective of the present article is to demonstrate an alternative method based on blade-element theory. This method is suitable for rapid estimation of impeller characteristics, when a full CFD simulation is not justified. The predictions are usually sufficient for engineering applications when only the impeller performance needs to be assessed. The approach is particularly beneficial when it is required to determine the effect of changing impeller geometry on the pumping velocity, tank wall velocity, and suspension of solids.

A resistance coefficient is required to determine the operating point of an impeller. The resistance characteristics (system curve) of a mixing tank is rather unique and it is different from that in a ducted impeller system (such as a ducted axial flow fan). Experimental calibration using LDV measurements was employed to determine the resistance coefficient in a standard mixing tank so that the impeller operating point could be found and the outlet velocity distribution could be predicted reliably for this geometry.

Measurements were carried out using a two-dimensional LDV system to characterize the velocity field produced by different axial-flow impellers in various mixing vessels.

Theoretical Formulations

Impeller outlet swirl-velocity distribution

An impeller can be characterized by a set of performance curves, that is, the head vs. flow, power vs. flow, and efficiency vs. flow curves. The performance of an axial flow can be analyzed by considering the flow in a cylindrical plane containing the two-dimensional flow field around the blade section, as shown in Figure 1. The cylindrical plane is located at a radial distance r from the axial and a small blade element of thickness Δr is analyzed. The flow in the impeller region is assumed to be two-dimensional, so that the radial velocity can be considered small and negligible for evaluating the lift and drag forces on the blade. The second assumption is that the blade solidity is small, which is usually the case for mixing-vessel impellers, so that interference between the blades can be neglected.

Referring to Figure 1b, the velocities at the inlet (denoted by a subscript 1) and the outlet (denoted by a subscript 2) of the airfoil include the absolute velocity V observed in the fixed frame of reference, the relative velocity W observed in the rotating frame of reference, and the impeller velocity U. To calculate the lift and drag forces, a mean relative velocity W_m is defined as

$$W_m = \sqrt{\frac{(V_{a1} + V_{a2})^2}{2} + \left(U - \frac{V_{\theta 1} + V_{\theta 2}}{2}\right)^2},$$

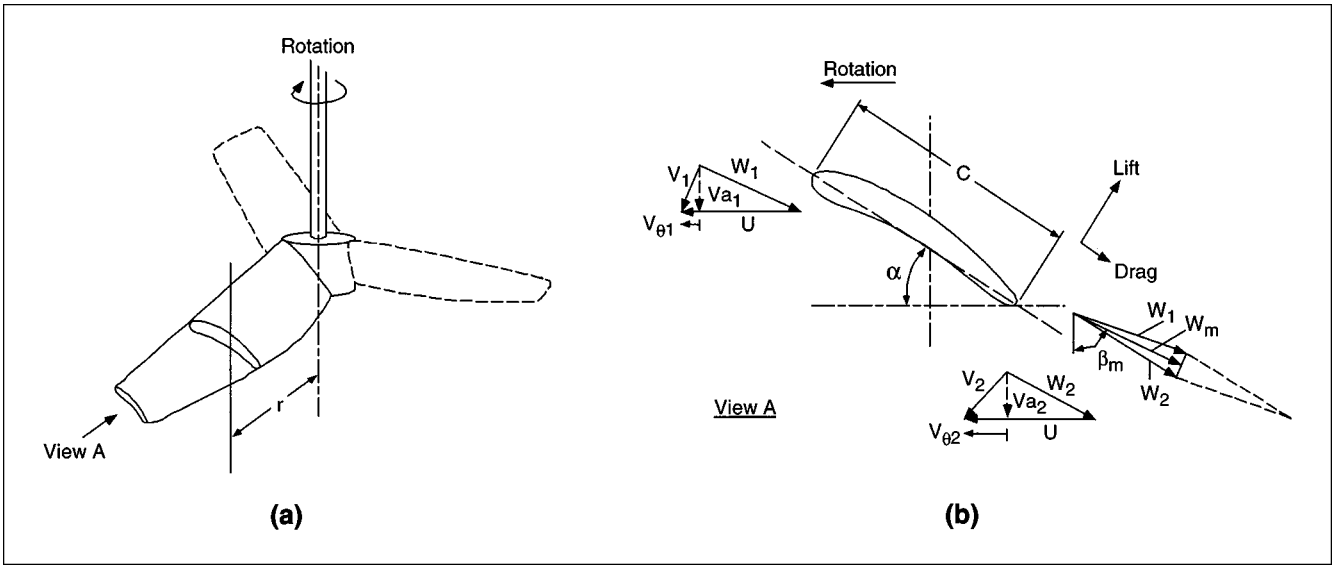

Figure 1. Blade-element analysis for an axial-flow impeller.

and the lift force can then be expressed as

$$L = \frac{1}{2} C_L \rho W_m^2 \Delta r c,$$

and the drag force as

$$D = \frac{1}{2} C_D \rho W_m^2 \Delta r c,$$

where c is the chord length of the blade section and ρ is the fluid density; C_L and C_D are lift and drag coefficients, respectively, which are a function of the angle of attack:

$$C_L = C_L(\Delta\alpha)$$
$$C_D = C_D(\Delta\alpha)$$

and the angle of the attack is

$$\Delta\alpha = \alpha - \left(\frac{\pi}{2} - \beta_m\right),$$

where β_m is the angle between the mean relative velocity vector and the vertical axis (Figure 1b). The total tangential force Y exerted by the blade section at radial position r is

$$Y = N_{bld}(L\cos\beta_m + D\sin\beta_m),$$

where N_{bld} is the number of the blades. This is equal to the change of the angular momentum:

$$Y = \rho 2\pi r \Delta r (V_{a2} V_{\theta 2} - V_{a1} V_{\theta 1})$$

Equating the two expressions and nondimensionalizing all the parameters gives:

$$\epsilon_{\theta 2} = \frac{\sigma}{2\cos\beta_m} \frac{(1+\Sigma)^2}{4} (C_L + C_D \tan\beta_m) + \epsilon_{\theta 1} \qquad (1)$$

$$\tan\beta_m = \frac{1/\lambda - (\epsilon_{\theta 1} + \epsilon_{\theta 2})/2}{(1+\Sigma)/2}, \qquad (2)$$

where

$$\epsilon_{\theta 1,2} = \frac{V_{\theta 1,2}}{V_a}, \qquad \Sigma = \frac{V_{a2}}{V_a}, \qquad \sigma = \frac{cN_{bld}}{2\pi r}, \qquad \lambda = \frac{V_a}{U},$$

$$V_a = \frac{4Q}{\pi(D^2 - d^2)}, \qquad V_{a1} \approx V_a,$$

where V_a is the area-averaged velocity (impeller bulk velocity), Q is the flow rate through the impeller, D is the impeller diameter, d is the hub diameter, Σ is the velocity shape function whose calculation will be discussed later, and σ is the blade solidity.

At any given radial position r, the nondimensional swirl-velocity distribution $\epsilon_{\theta 2}$ at the impeller outlet plane can be found by iterations using Eqs. 1 and 2. The present technique uses an iteration scheme starting from an estimated β_m. The swirl velocity (Eq. 1) is then calculated and β_m (Eq. 2) updated. The iteration continues until convergence is achieved. Convergence is usually achieved within 6 or 7 iterations—an error less than 0.02 degrees for β_m.

Lift and drag coefficients (C_L and C_D) are dependent on blade-section geometry, Reynolds number, and the angle of attack. Data for a wide range of blade sections can be found in Abbot and Von Doenhoff (1959), Selig et al. (1989), and Wallis (1983).

Impeller energy head distribution

Once the swirl-velocity distribution at the impeller outlet is found, the energy rise (head) at the radial position r can be found:

$$H(r) = \rho\overline{\omega}(V_{\theta 2} r_2 - V_{\theta 1} r_1) - \Delta H_R, \qquad (3)$$

where ΔH_R is the impeller's hydraulic loss and can be calculated by (Wallis, 1983)

$$\Delta H_R = \frac{1}{2}\rho V_a^2 C_D \frac{\sigma(1+\Sigma)^2}{4\cos^3\beta_m}.$$

The total impeller's head rise can be found from integration:

$$H = \frac{\int_{R_b}^{R_t} H(r) r \Sigma \, dr}{\int_{R_b}^{R_t} r \Sigma \, dr}.$$

The H vs. Q curve is most usefully expressed in a nondimensional form:

$$N_H = \frac{H}{\rho N^2 D^2}$$
$$N_Q = \frac{Q}{ND^3},$$

where N_H and N_Q are head and flow numbers, respectively.

The shaft power can be found from

$$P = (H + \Delta H_R) Q,$$

or in a nondimensional form:

$$P_0 = \left(N_H + \frac{\Delta H_R}{\rho N^2 D^2}\right) N_Q,$$

where P_0 is the power number and is defined as

$$P_0 = \frac{P}{\rho N^3 D^5}.$$

Tank bulk flow resistance

The pumping rate and power consumption of an impeller operating in a mixing vessel depends on flow resistance as well as the impeller performance. The flow resistance (ΔH) within a mixing vessel takes the approximate form:

$$\Delta H \propto \rho V_a^2,$$

or, in a nondimensional form:

$$\frac{\Delta H}{\rho N^2 D^2} = R N_Q^2, \tag{4}$$

where R is the resistance coefficient and is usually a function of mixing-vessel geometry and flow generalized Reynolds number (Re). (Note: For laminar flows, suspension flows, or viscoplastic fluids with a substantial yield stress, this relationship is more complex.) At high Reynolds number, R is independent of Re. The intersection of the resistance curve and the impeller-head curve gives the operating point of the impeller operating in the mixing vessel. R can be determined experimentally by measuring the N_Q of an impeller with its performance known (that is, calculated using the present technique).

Impeller outlet-velocity shape function

The impeller spanwise head distribution is equal to the flow-resistance distribution:

$$H(r) = \xi \rho V_{a2}^2(r),$$

where ξ is the energy loss coefficient, which is usually a function of radius r, mixing vessel geometry, and fluid rheology, but is insensitive to the impeller geometry. ξ can be found from velocity data obtained through LDV measurements to be described later. The velocity shape function can then be calculated:

$$\Sigma = \frac{V_{a2}}{V_a} = \frac{1}{V_a}\sqrt{\frac{H(r)}{\xi \rho}}\ . \tag{5}$$

Clearly, to calculate the head distribution $H(r)$, a prior knowledge of the swirl-velocity distribution, which is a function of the velocity shape function, Σ is required. To solve this, an iteration on Σ using Eqs. 3 and 4, together with the iterative scheme for solving Eqs. 1 and 2, has been implemented. Convergence to 0.5% is usually achieved with 10 iterations of this outer loop.

Experimental Equipment

The model mixing rig (Figure 2) consists of a $T = 1{,}070$ mm diameter and 1,800 mm high circular tank with a flat bottom placed inside a rectangular outer glass tank. This outer tank is filled with water to minimize the optical distortion. Four baffles $1/12$ T in width and equally spaced were installed in the circular tank. Test impellers were mounted on a central shaft equipped with an Ono Sokki torque transducer and optoelectronic speed detector. The speed of this shaft could be varied from 0 to 600 rpm by means of a variable frequency drive. The speed and torque were logged using a 486 PC equipped with a suitable data-acquisition board, and pro-

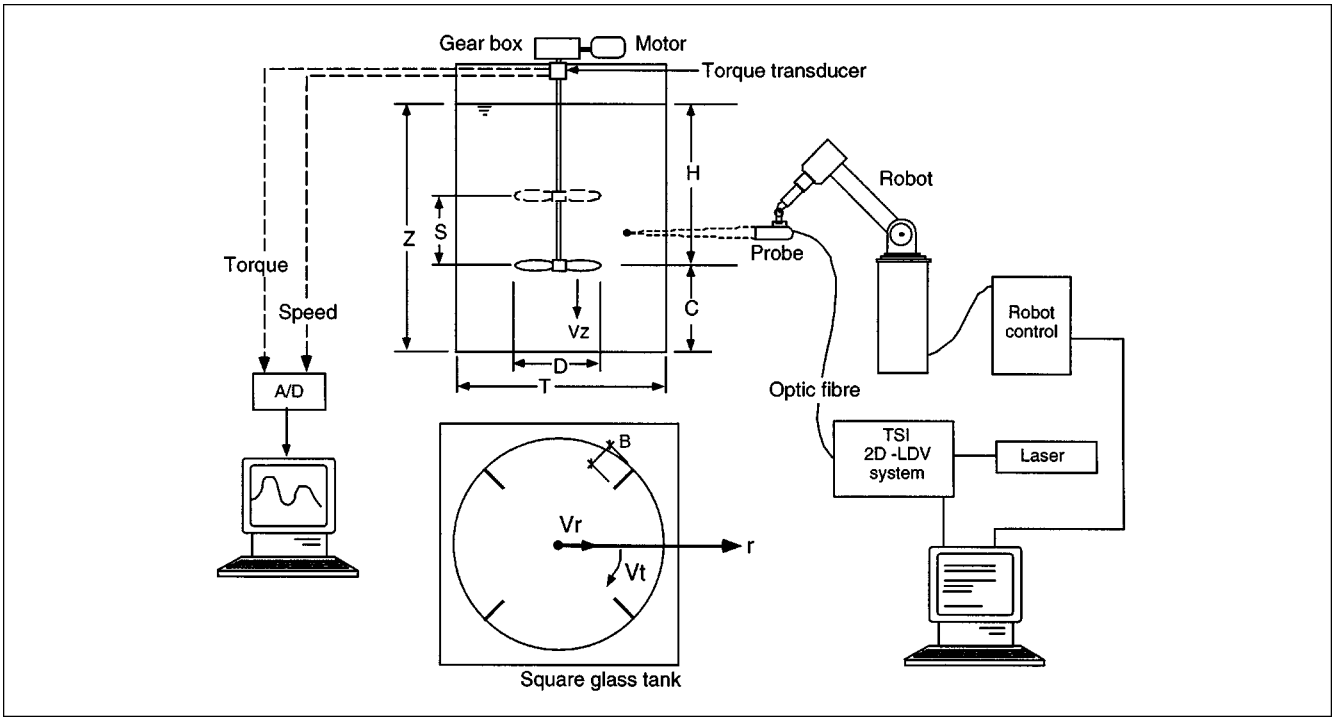

Figure 2. Model mixing tank located at CSIRO.

The optical-fiber probe of the TSI LDV system was traversed automatically by a robotic arm.

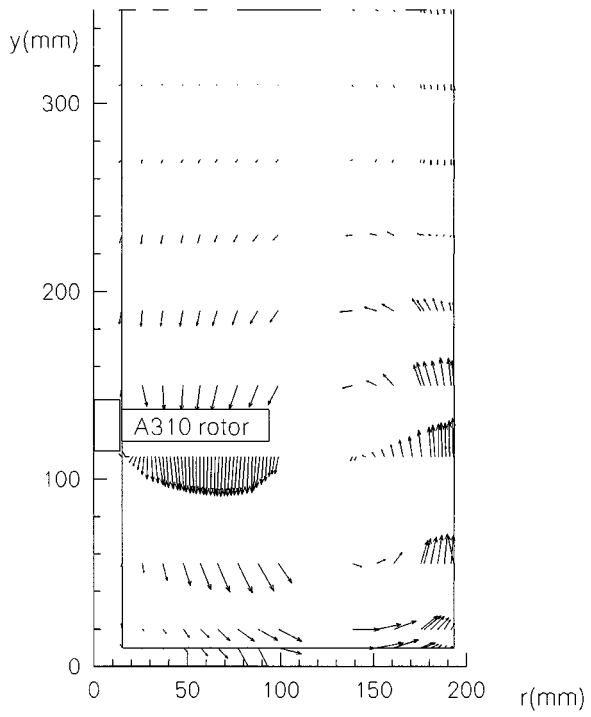

Figure 3. Time-mean velocity vector field.

Impeller: a three-bladed Lightnin A310; $C/T = 1/3$, $B/T = 1/12$, $D/T = 0.47$. Fluid: water, shaft speed $N = 300$ rpm, $Re = 477{,}000$.

vided on-line analysis of power consumption, and so on. Detailed geometrical parameters are defined in the diagram. A geometrically similar but smaller mixing tank (with $T = 390$ mm) was also used in the experiments. This enabled the scaling effect for the impeller pumping velocity field to be studied.

Velocity distributions were measured in the model mixing vessels using a TSI two-dimensional optical-fiber LDV system. The transmitting and receiving optics of this probe were mounted on an industrial robotic arm, allowing the probe to be automatically positioned within the tank. Because of the irregular sampling nature of the LDV method, bias correction had to be used to calculate time-mean statistics. The time-mean velocity data thus obtained were found repeatable to within 1%. Time-mean statistics of the velocity data were obtained using a time-weighted bias-correction method incorporated in the TSI package.

Results

Experimental results

Measurements were carried out for different fixed-geometry axial-flow impellers, and one axial-flow impeller with adjustable blade setting angle was also used in the experiment. A typical velocity distribution is shown in Figure 3 where velocity vectors are plotted in an axial plane located midway between the baffles. The fluid used was water, and the impeller Reynolds number based on the shaft speed and the impeller diameter was $Re = \rho ND^2/\mu = 477{,}000$.

The axial velocity profiles at a position just underneath the axial flow impeller (5% T below the impeller centerline) are plotted in Figure 4 over a C/T range of 0.2−0.46 for $D/T = 0.42$. Not shown here are the measurements repeated over a D/T range of 0.35−0.5. The axial pumping flow rate Q of an impeller was calculated by integrating the axial velocity distributions from the shaft axis to the impeller tip, similar to the approach used by Jaworski et al. (1991). The flow number was then found from $N_Q = Q/(ND^3)$. This process was repeated for a range of axial-flow impellers, over a range of different impeller solidity and impeller-blade setting angles. Flow-number variation with C/T and D/T for a Lightnin A310 impeller is shown in Figure 5. The data thus collected were used to calculate the tank resistance coefficients (refer to Eq. 4). The resulting tank resistance curve is shown in Figure 6a; the resistance coefficient = 1.32 for $D/T = 0.42$, $C/T = 1/3$.

Performance analysis: Code validation

A Win32 computer program based on the formulations described earlier was developed (Pullum et al., 1998). Included in this software are also lift and drag coefficients for a wide range of generalized Reynolds numbers. Typically, only a fraction of a second is needed to calculate the performance of an impeller using this code for operating on a Pentium PC.

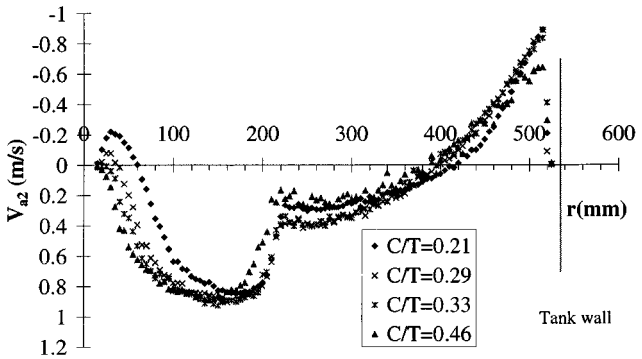

Figure 4. Time-mean axial-flow velocity distribution underneath a downward A310 impeller; $D = 452$ mm ($D/T = 0.42$), $N = 140$ rpm.

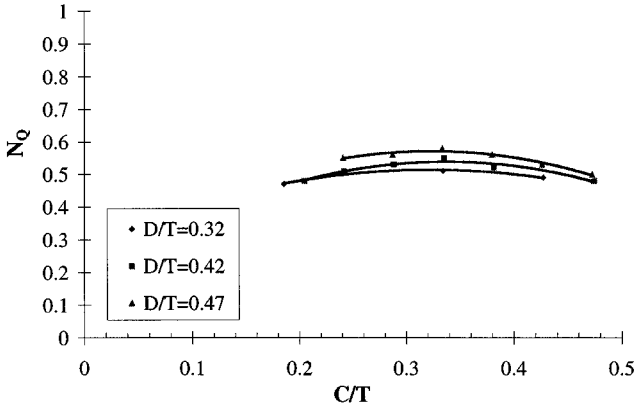

Figure 5. Flow-number variation with D/T and C/T parameters.

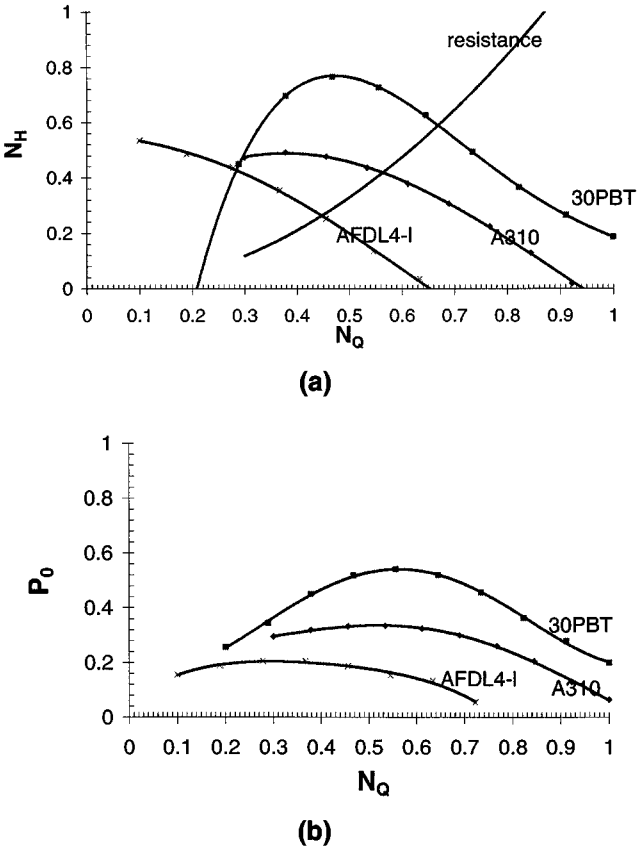

Figure 6. Performance evaluation of axial-flow impellers operating in mixing vessel: (a) head-number curve; (b) power-number curve.

Reynolds number is assumed to be sufficiently high so that flow is turbulent. The resistance curve was obtained using LDV data and found valid for $D/T = 0.35–0.5$.

Typical performance curves for high Reynolds number flows, predicted using *Agitator*, are plotted in Figure 6a and 6b for three impellers: Lightnin A310 (a three-bladed axial-flow impeller). AFDL4-1 (a high-efficiency four-bladed impeller, with the blade angled at 10° at the tip and 34° at the hub), and a 30° pitched-blade turbine (30PBT, with the blade width equal to $D/5$). The impellers are located at $C = T/3$ from the tank bottom. The intersections of the resistance curve and the head curves (Figure 6a) determine the points at which the impellers actually operate. The flow number at which an impeller operates can be found at the intersection point (Figure 6a). The three axial-flow impellers show different performance and different operating flow numbers. It can also be seen that impellers with a large head number consume more power (Figure 6a and 6b). A head curve usually exhibits a peak at an optimal flow number. At high flow numbers, the flow past a blade section produces a small angle of attack, which results in a reduction in the lift force, hence the head, while at small flow numbers, the angle of attack of the flow becomes too high, resulting in flow separation and blade section stalls. The intersection of the resistance curve with the head curve is where the head generated by an impeller just balances the resistance required to drive the flow circulation.

The axial velocity distribution below the three impellers was measured using the LDV system in the model mixing tank (Figure 2), and their nondimensional time-mean velocities are plotted in Figure 7. It can be concluded that predictions are in good agreement with measurements. It is interesting to note that impeller 30PBT produces the least even velocity profile. This is expected, as the spanwise loading distribution of the impeller is highly uneven, due to a large angle of attack at the tip and a small angle of attack at the hub of the impeller. The velocity profiles are also predicted by *Agitator* to a reasonable degree of accuracy. By comparison, more uniform velocity profiles are produced by the other two impellers (A310, AFDL4-1), as these two impellers have twisted blades such that the angle of attack distributions are more uniform, and hence the loading distribution is more even.

The flow numbers integrated from the velocity profiles and predictions (as shown in Figures 6a and 6b) are listed in Table 1, together with the power numbers measured with the torque transducers. Good agreement between predictions and measurements can be seen. Although not shown in this article, the flow numbers of many other axial flow impellers were also measured in our laboratory and compared well with predictions. In general, predictions were found within 5–10% of measurements. Figure 8 shows the variation of power number with blade angle predicted using the code. A modified A310 impeller capable of varying the blade angle was used for this measurement. The results are in good agreement with prediction (Figure 8).

Performance analysis: Impeller geometry influence

Using *Agitator*, it is possible to rapidly estimate the influence of various parameters on the impeller performance. A CSIRO axial-flow impeller (AFDL4) has been used to investigate the blade angle and the number of blades on the impeller performance. AFDL4 has a blade width-to-diameter ratio of 0.11 at the tip and 0.19 at the hub, and a blade setting angle of 13° at the tip and 36° at the hub. For the purpose of illustration, turbulent flow is assumed, and $C/T = 1/3$ and $D/T = 0.4$. Figure 9 shows the flow-number variation

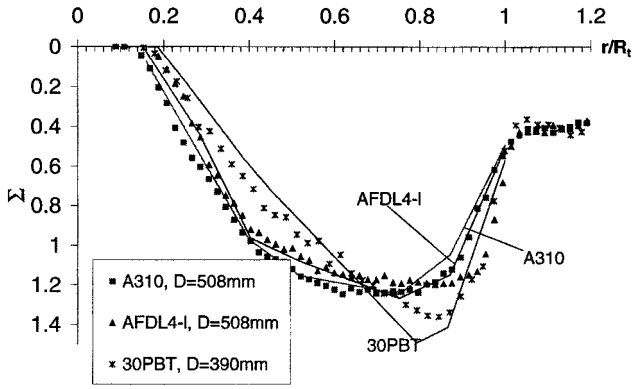

Figure 7. Time-mean axial-velocity distribution at the impeller outlet: curves—predictions; points—LDV measurements.

All tests were conducted in water with impellers set at a shaft speed of 140 rpm. The impellers were installed at $C/T = 1/3$ from the tank bottom.

Table 1. Comparison of Prediction and Experiments*

Impellers	N_Q Calc.	N_Q Meas.	P_0 Calc.	P_0 Meas.
Lightnin A310	0.56	0.56	0.33	0.31
AFDL4	0.55	0.56	0.32	0.30
AFDL4-1 (low angle)	0.45	0.45	0.19	0.16
Four-bladed 30PBT	0.67	0.64	0.51	0.52

*$C/T = 1/3$, $D/T = 0.43$.

with the blade angle for two different blade numbers. Flow number increases with the blade setting angle α, but the rate of increase decreases as α increases. For a blade number of 4 ($N_{bld} = 4$), a maximum $\alpha = 19°$ exists beyond which flow number decreases as α increases. This maximum in α corresponds to a point where the blade stalls due to a large flow angle of attack. This maximum value of α reduces when the number of blades is decreased (the maximum $\alpha = 12°$ at $N_{bld} = 2$). This is expected, as a reduction in the number of blades results in a reduction of the axial velocity. This increases the angle of the attack β_m (Figure 1), resulting in an early stall of the blade section.

The variation of N_Q, P_0, $\epsilon_{\theta 2}$, and N_F with the number of blades and the blade angle are plotted in Figures 10a and 10b, where $\epsilon_{\theta 2}$ is the relative swirl velocity at the impeller exit ($= V_{\theta 2}/V_a$, Figure 1), and N_F is the nondimensional impeller thrust [$= F/(\rho N^2 D^4)$], where F is the thrust acting on the impeller]. In general, while the power number (P_0) shows a steady increase at increasing blade angle, the flow number (N_Q) and the thrust number (N_F) show a decreasing rate of increase for the reason just given. The impeller outlet nondimensional swirl velocity $\epsilon_{\theta 2}$ exhibits a minimum at $\alpha \approx 0$; $\epsilon_{\theta 2}$ increases as α varies from 0. This implies that if the blade angle is set too high or too low, the swirl velocity at the exit of an impeller becomes large, and this will result in large radial velocity. If this effect is significant, the impeller is deemed to be a mixed-flow or radial-flow impeller. For instance, a 45° pitched-blade turbine produces a mixed-flow pattern (that is, it produces both axial and radial velocities).

The effect of varying the blade number is shown in Figure 10b. All four parameters (N_Q, P_0, $\epsilon_{\theta 2}$, and N_F) increase with an increase in blade number. The increase with increasing blade-number levels out at large blade number; this is partic-

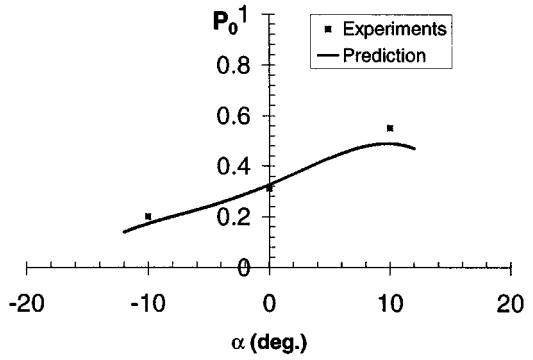

Figure 8. Power-number variation with blade angle.

The zero angle corresponds to the standard design of the impeller. Impeller: Lightnin A310; $C/T = 1/3$, $D/T = 0.42$.

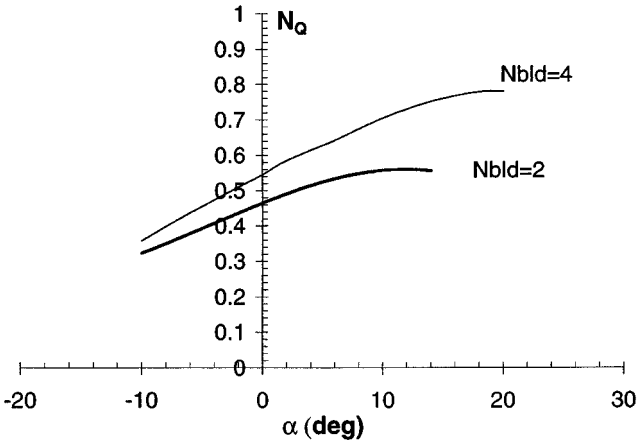

Figure 9. Variation of impeller flow number with blade setting angle.

N_{bld} is the number of the blades. Impeller: the CSIRO AFDL4 axial-flow impeller.

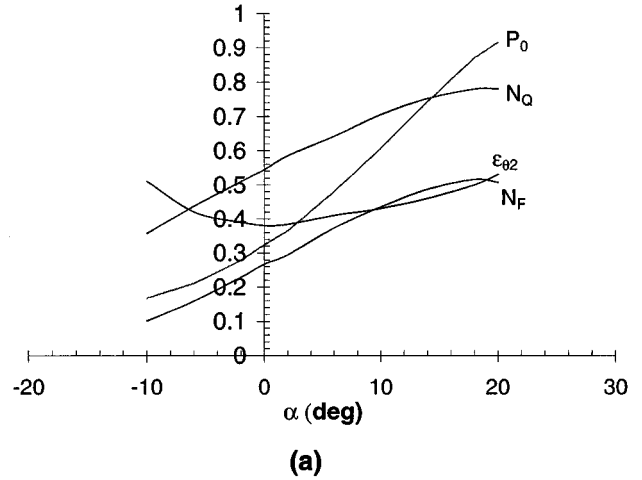

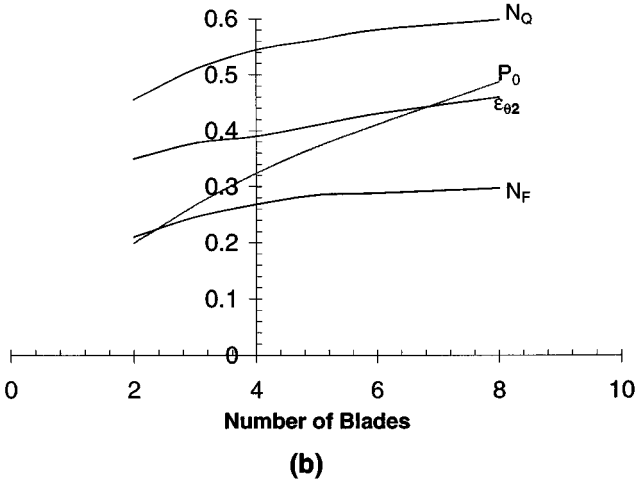

Figure 10. Influence of impeller geometry on impeller pumping performance: (a) influence of blade-setting angle; (b) influence of blade number.

Impeller used for the calculation was the CSIRO AFDL4 axial-flow impeller, which has a flow number of $N_Q = 0.55$ and P_0 of 0.29 for its standard configuration (four blades).

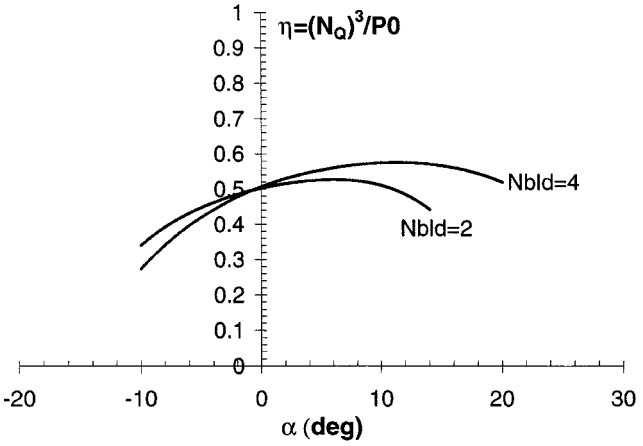

Figure 11. Impeller efficiency variation with impeller-blade angle.

ularly pronounced with the curves of N_Q and N_F. As a consequence, one cannot expect to double the pumping velocity if the number of the blades is doubled. This can be interpreted by analyzing the velocity triangles drawn in Figure 1b. It can be seen that the axial-velocity components (V_{a1} or V_{a2}) increase as the blade number increases; this results in a smaller β_m for the velocity (W_m) relative to the blade, hence a reduction in the angle of the attack.

It should be pointed out that the parameter that actually controls the impeller performance is the blade solidity ($\sigma = cN_{bld}/(2\pi r)$), as evident from Eq. 1. The effect of varying the blade number (N_{bld}) is identical to that of the blade chord (c), since both are related to the blade solidity in the same way.

Impeller efficiency analysis

To compare impellers in terms of pumping efficiency, the pumping flow rate produced at a given power input should be used for constant impeller diameter. It can be shown that

Table 2. Comparison of Impeller Efficiencies*

Impeller	Prediction $\eta = N_Q^3/P_0$	Measurement $\eta = N_Q^3/P_0$
Lightnin A310	0.567	0.58
A310 with dia. cut by 11%	0.54	0.57
Lightnin A410	0.562	0.56
AFDL4	0.563	0.57
30PBT	0.490	0.504
45PBT	—	0.388

*$C/T = 1/3$ and $D/T = 0.43$. Pumping Direction: Downward.

$$Q^3 = \left(\frac{N_Q^3}{P_0}\right)\frac{p}{\rho}D^4.$$

Thus, the coefficient (N_Q^3/P_0) determines the pumping efficiency. The parameter was used by Jaworski et al. (1996), among others, in evaluating the impeller circulation efficiency of axial-flow impellers. Figure 11 shows the variation of impeller efficiency with blade setting angle. Clearly, the impeller efficiency is a function of the blade angle and the number of blades. An optimum angle exists in achieving the maximum impeller efficiency.

Table 2 shows a comparison of different axial-flow impellers in terms of impeller efficiency. A standard Lightnin A310 impeller, a modified A310 (cut by 11% in its diameter), a Lightnin A410 with three blades of large solidity and setting angle, the CSIRO AFDL4, and pitched blade turbines (30° and 45°) were used for comparison. It is interesting to note that other than the pitched-blade turbines (30PBT, 45PBT), all the other axial-flow impellers have almost equal efficiency. The pitched-blade turbines have lower efficiency.

Performance analysis: Blade-section profile influence

Two important geometric factors controlling the blade section aerodynamics are the blade camber (b/c) and the blade thickness (t/c). The defintion of b/c and t/c are shown in Figure 12, where b is the camber height, t is the maximum

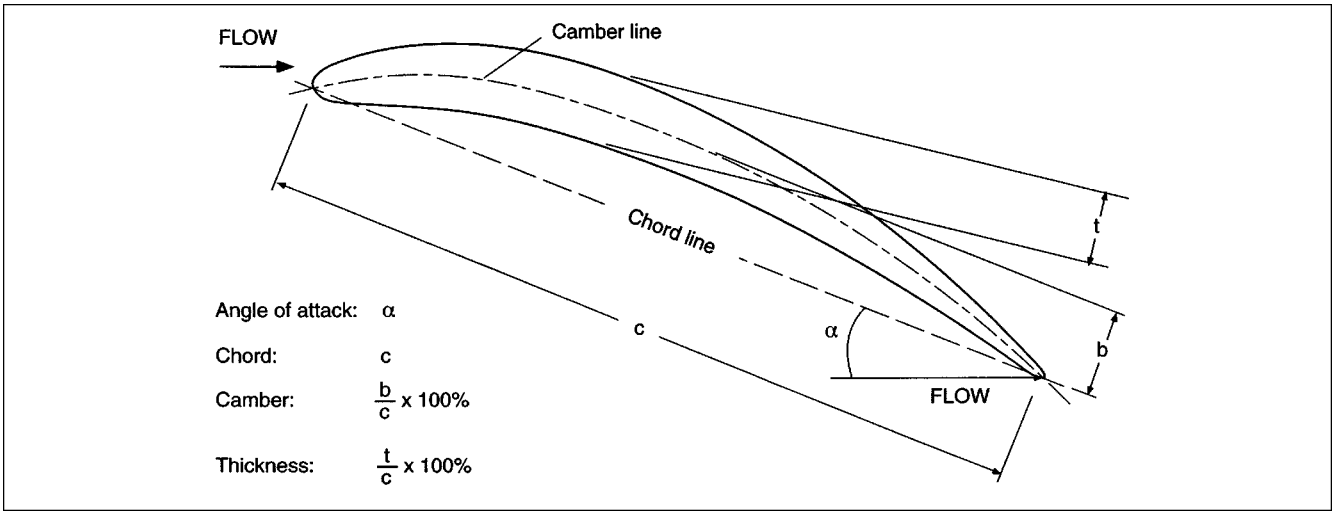

Figure 12. Blade section geometry.

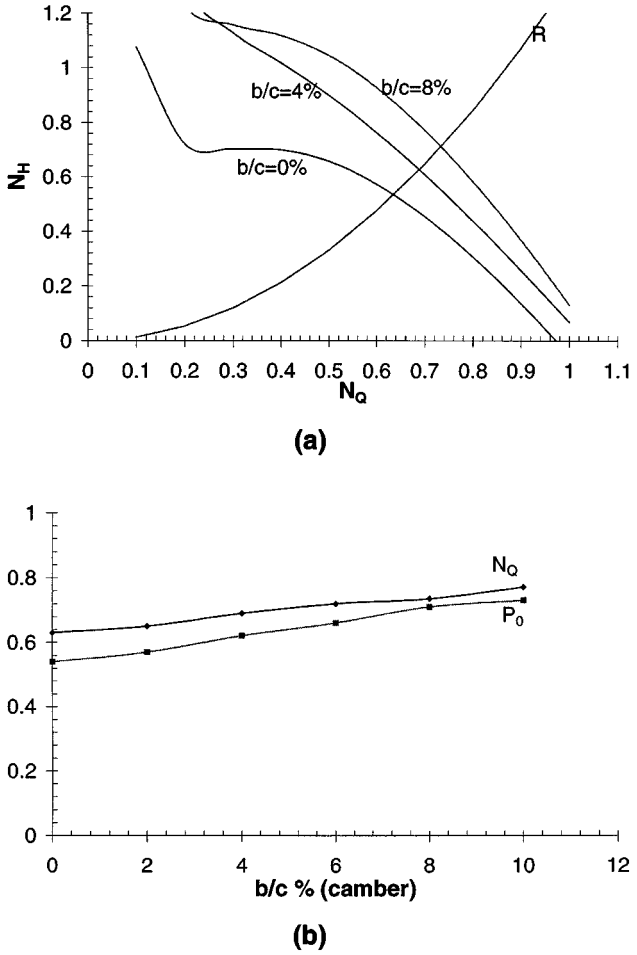

Figure 13. Influence of blade section geometry impeller pumping performance: (a) head vs. flow-number curves at different blade chamber; (b) flow-number and power-number variation with blade chamber.

blade thickness, and c is the blade chord length. As a first approximation, the aerodynamics of a blade section of arbitrary design can be approximated by an arc-shaped blade section with the same b/c and t/c. The influence of the blade section on impeller performance can be predicted using experimentally obtained lift and drag coefficients with b/c and t/c. The correlation of C_L and C_D with blade section can be found in Wallis (1983) or Abbott and Von Doenhoff (1959).

The influence of camber on impeller performance is plotted in Figure 13a and 13b for the CSIRO AFDL4 impeller. Figure 13a shows that as b/c increases, the head curves increase, resulting in an increase in the operating flow number (determined at the intersection points). The flow number increased from $N_Q = 0.63$ to 0.77 as b/c is increased from 0 (that is, flat plate) to 10%, while the power number increased from 0.54 to 0.73 (Figure 13b). Modification of b/c can be useful if a large flow number is required when a further increase of the blade angle cannot be used. Figure 14 shows the efffect of varying blade thickness. As the blade thickness is increased from $t/c = 3\%$ to 10%, the flow number reduced from 0.73 to 0.71, that is, a 3% reduction. From considera-

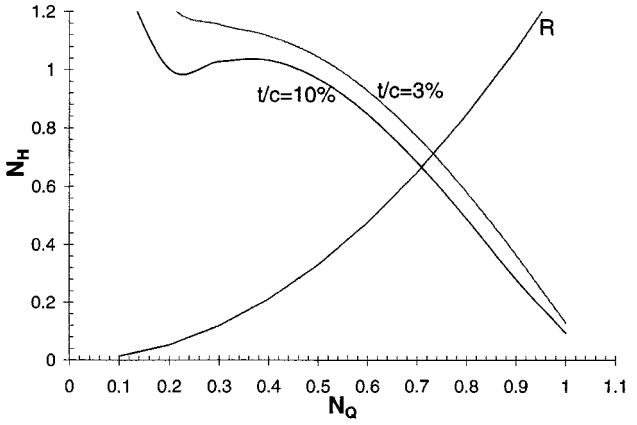

Figure 14. Influence of blade thickness on impeller performance.

The head curves at two different blade thickness. The curve labeled R is the resistance curve.

tions of turbulent length scales, Buurman et al. (1986) have shown that the blade thickness plays a role in scaling-up solids suspension data. The present result shows that the blade thickness also influences the pumping velocity, possibly having a more direct effect on suspension capabilities.

Discussion

The advantage of the present approach is that the pumping performance of an impeller in a mixing vessel can be found rapidly. The influence of the impeller geometry can be estimated to a good degree of accuracy. The present technique is particularly useful if one wishes to compare different axial flow impellers. The technique can also be used to examine the performance of newly designed impellers or retrofitting an existing impeller.

The technique can also be used to estimate the swirl- and axial-velocity profiles at the impeller outlet. This can be extremely useful if one wishes to calculate the velocity field over the whole mixing tank using CFD techniques. The velocity information obtained using the present technique can be used as an input to the CFD simulation. This obviates the need to use more elaborate and costly approaches such as the sliding mesh method (Koh and Wu, 1998). An application of this approach is described by Niclasen et al. (1997).

The emphasis of the present study is on the prediction of the influence of impeller design variables on the pumping flow number, power number, swirl velocity, and so on. These variables are important in determining suspension of solids and dispersion of gas. Future work is needed to further correlate the predicted variables to parameters such as the S value in Zwietering's correlation (Zwietering, 1958). It is also possible to examine the effect of fluid viscosity, provided that the dependence of the lift and drag coefficient on Reynolds number is given.

The present technique is based on the axial-flow assumption. This is valid if only a small amount of the radial-velocity component exists, as only the axial- and tangential-velocity components are used in calcultaing the lift and drag. If the swirl velocity at the impeller outlet is sufficiently large (due to, for example, large blade solidity, or large blade setting

angle), the flow leaving the impeller becomes radial. When this happens, the present technique is no longer valid as the centrifugal force will contribute to the pumping. Without going into much detail, it was found duirng our study that the amount of the radial-velocity component is proportional to $(V_\theta/V_a)^2$. Further work is needed to predict the swirl-induced radial velocity.

Conclusions

Theoretical formulations are presented to evaluate the performance of mixing-vessel axial-flow impellers. A computer code *Agitator* thus developed has been used to calculate the head number and power number vs. flow number of different axial flow impellers. The calculations were found to be in good agreement with experiments. It is also demonstrated that the code can be used to predict an impeller-outlet velocity profile and to estimate the influence of various parameters on impeller performance.

Variation of impeller flow number, power number, and many other parameters with impeller-blade angle and blade solidity is illustrated using the present technique. While the power number shows a steady increase at increasing blade angle, the flow number and the thrust number show a decreasing rate of increase. The flow, power, thrust, and swirl numbers increase with an increase in blade number. The increase with increasing blade number levels out at a large blade number; this is particularly pronounced with the curves of the flow number and thrust number. As a consequence, one cannot expect to double the pumping velocity if the number of the blades is doubled. The flow number is reduced as the blade thickness is increased.

Acknowledgment

The authors acknowledge the support from AMIRA P419 project sponsored by the following companies: Lightnin Mixers, Queensland Alumina Limited, Alcoa of Australia, Comalco Aluminium, RGC Mineral Sands Ltd., Westralian Sands Ltd., BOC Gases, Placer Pacific, Normandy Mining, Western Mining Corporation.

Notation

C = impeller-to-tank floor distance, mm
H = impeller head, Pa
N = shaft speed, r/s, rpm
N_{js} = just suspension speed, rpm
R_t = impeller tip radius, mm
T = tank diameter, mm
V = absolute velocity, m/s
V_θ = tangential velocity, m/s
ΔH = tank head loss, Pa
$\epsilon_{\theta 2}$ = impeller outlet swirl velocity, normalized by V_a
η = pumping efficiency
Σ = normalized axial velocity
ω = impeller angular speed, rad/s

Literature Cited

Abbott, I. H., and A. E. Von Doenhoff, *Theory of Wing Sections*, Dover, New York (1959).
Buurman, C., G. Resoort, and A. Plaschkes, "Scaling-Up Rules for Solids Suspension in Stirred Vessels," *Chem. Eng. Sci.*, **41**(11), 2865 (1986).
Downie, R. J., M. C. Thompson, and R. A. Wallis, "An Engineering Approach to Blade Designs for Low to Medium Pressure Rise Rotor-Only Axial Fans," *Exp. Thermal and Fluid Sci.*, **6**, 376 (1993).
Hutchings, B. J., R. J. Weetman, and R. P. Bharatan, "Computation of Flow Fields in Mixing Tanks with Experimental Verification," *Proc. ASME Winter Meeting*, San Francisco, CA (1989).
Jaworski, J., A. W. Nienow, and N. K. Dyster, "An LDA Study of the Turbulent Flow Field in a Baffled Vessel Agitated by an Axial, Down-Pumping Hydrofoil Impeller," *Can. J. Chem. Eng.*, **74**, 3 (1996).
Jaworski, Z.., A. W. Nienow, E. Koutsakos, K. Dyster, and W. Bujalski, "An LDA Study of Turbulent Flow in a Baffled Vessel Agitated by a Pitched Blade Turbine," *Chem. Eng. Res. Design*, **64**(A4), 313 (1991).
Koh, P. T. L., and J. Wu, "CFD Simulation of Flow in Mechanically Stirred Tanks with Fluidfoil Impellers," *Proc. Chemeca 98*, Port Douglas, Australia (1998).
Lee, K. C., and M. Yianneskis, "Turbulence Properties of the Impeller Stream of a Ruston Turbine," *AIChE J.*, **44**(1), 13 (1998).
Lewis, R. I., *Turbomachinery Performance Analysis*, Arnold, London (1996).
Niclasen, D. A., M. Rudman, H. M. Blackburn, and J. Wu, "Flow Simulation of a Mixing Vessel Incorporating Blade Element Theory," *Proc. Int. Conf. on CFD in Mineral & Processing & Power Generation*, Melbourne, Australia, p. 395 (1997).
Nouri, J. M., and J. H. Whitelaw, "Flow Characteristics of Stirred Reactors with Newtonian and Non-Newtonian Fluids," *AIChE J.*, **36**(4), 627 (1990).
Pullum, L., J. Wu, and P. I. Cooper, "Agitator: A New Windows Based Tool for the Design and Evaluation of Mixing Tanks Using Axial Flow Impellers," *Proc. Chemeca 98*, Port Douglas, Australia (1998).
Selig, S. M., J. F. Donovan, and D. B. Fraser, *Airfoils at Low Speeds*, Stokely, London (1989).
Wallis, R. A., *Axial Flow Fans and Ducts*, Wiley–Interscience, New York (1983).
Weetman, R. J., "Development of Transitional Flow Mixing Impellers," *Proc. 7th Eur. Conf. Mixing*, Brugge, Belgium (1991).
Weetman, R. J., "Automated Sliding Mesh CFD Computations for Fluidfoil Impellers," *Proc. Eur. Conf. on Mixing*, Paris, France (1997).
Weetman, R. J., and J. Y. Oldshue, "Power, Flow and Shear Characteristics of Mixing Impellers," *Proc. 6th Eur. Conf. on Mixing*, Pavia, Italy (1988).
Wu, J., L. Pullum, M. Welsh, and R. Yunken, "Rapid Diagnosis of Flow Separation Around an Axial Impeller in a Mixing Vessel," *Exp. Fluids*, **22**(6), 519 (1997).
Yianneskis, M., Z. Popiolek, and J. H. Whitelaw, "An Experimental Study of the Steady and Unsteady Flow Characteristics of Stirred Reactors," *J. Fluid Mech.*, **175**, 537 (1987).
Zwietering, T. N., "Suspending of Solid Particles in Liquid by Agitators," *Chem. Eng. Sci.*, **8**, 244 (1958).

Manuscript received Mar. 8, 1999, and revision received Oct. 25, 1999.